Carbon dioxide (CO_2) fracturing of volcanic rocks under geothermal conditions

Kohei Takuma, Yuto Watanabe, Kiyotoshi Sakaguchi, Noriaki Watanabe
Tohoku University, Sendai, Japan

Kazumi Osato
Geothermal Energy Research and Development Co., Ltd. (GERD), Tokyo, Japan

Amane Terai
Japan Organization for Metals and Energy Security (JOGMEC), Tokyo, Japan

ABSTRACT: An enhanced geothermal system that uses carbon dioxide (CO_2) for both reservoir creation and thermal energy extraction has been attracting attention in Japan. For this system, CO_2 fracturing is conducted to create highly permeable fractures in low-permeability reservoirs, for instance, consisting of volcanic rocks. However, there is no previous study on CO_2 fracturing of volcanic rocks under geothermal conditions, and possibility and characteristics of such fracturing are therefore unknown. Here we present results of CO_2 fracturing experiments on andesite and basalt at 250 °C and a confining pressure of 30 MPa. It is demonstrated that CO_2 fracturing occurs at a lower pressure than water fracturing and produces a more complex fracture pattern with a substantial permeability improvement. Additionally, it is shown that CO_2 fracturing with water, in which CO_2 is chased and pressurized by water, can produce larger-aperture fractures (i.e., larger permeability improvement) with keeping the advantage in CO_2 fracturing.

Keywords: carbon dioxide, fracturing, volcanic rock, enhanced geothermal system, breakdown pressure, fracture pattern.

1 INTRODUCTION

An enhanced geothermal system that uses carbon dioxide (CO_2) for both reservoir creation and thermal energy extraction has been attracting attention in Japan. For this system, CO_2 fracturing is conducted to create highly permeable fractures in low-permeability reservoirs, for instance, consisting of volcanic rocks.

However, to the best of the authors' knowledge, few laboratory CO_2 fracturing experiments have been conducted using CO_2 and geothermal conditions to date (Isaka et al., 2019; Pramudyo et al., 2021; Pramudyo et al., 2023). Additionally, there is no previous study on CO_2 fracturing of volcanic rocks under geothermal conditions, and possibility and characteristics of such fracturing are therefore unknown. In this context, the present study aimed at clarifying possibility and characteristics of CO_2 fracturing on volcanic rocks under geothermal conditions. This paper presents results of CO_2 fracturing experiments on andesite and basalt at 250 °C and a confining pressure of 30 MPa.

2 MATERIALS AND METHODS

Cylindrical rock samples (diameter, 30 mm; length, 25 mm) with a single borehole (diameter, 1.5 mm; length, 10 mm) were prepared using Genbudo basalt from Hyogo prefecture, Japan, and Honkomatsu andesite from Kanagawa prefecture, Japan. X-ray computed tomography (CT) and permeability measurements were conducted on each sample before and after the experiment. The X-ray CT was carried out under dry, room temperature, and atmospheric pressure conditions at an X-ray tube voltage of 120 kV, a tube current of 150 µA, and a voxel size of 25 µm × 25 µm × 25 µm, to confirm formation of fractures. The permeability of the sample was measured in a radial flow geometry at room temperature and atmospheric pressure, by injecting water into the borehole with graphite gaskets.

Figure 1 shows the experimental system used in the present study, which uses a special triaxial cell (Watanabe et al., 2017a; Watanabe et al., 2017b; Watanabe et al., 2020; Goto et al., 2021; Pramudyo et al., 2021; Watanabe et al., 2021; Pramudyo et al., 2023). The triaxial cell employs a high-viscosity plastic melt as a confining fluid, and a 50-µm thick plastic (polyimide) film as a sleeve for the sample. The plastic melt in this study was polyethylene (PE) melt. PE melts at 120–140 °C, and decomposes at ~370 °C. The polyimide film does not have a melting point. It decomposes before melting at > 500 °C. A tube with a PE rod, which injects PE melt at the experimental temperature, was attached to the upper part of the cell. The PE melt injection provides confining pressure and is controlled using a metallic piston that is displaced by pumping water at a constant pressure. The axial pressure in the triaxial cell is provided by two cylindrical pistons with an axial hole for fluid flow. The piston positioned at the injection side is equipped with an injection pipe connected to a syringe pump. The axial load is applied by a hand pump-operated hydraulic jack that displaced the piston on the production side. Axial pressure is applied to the sample through a copper gasket placed between the piston and the end face of the sample, where only gasket at the injection side had a hole. Acoustic emission (AE) measurements can be conducted to determine the breakdown pressure during fluid injection using an AE measurement device (Physical Acoustics Cooperation's two-channel data acquisition and digital signal processing AE system, PCI-2) with an AE sensor (R15α 150-kHz resonant frequency sensor, Physical Acoustics Corporation). The AE device with the sensor gathers acoustic signals through axial load pistons, an amplifier, and a computer for recording and processing.

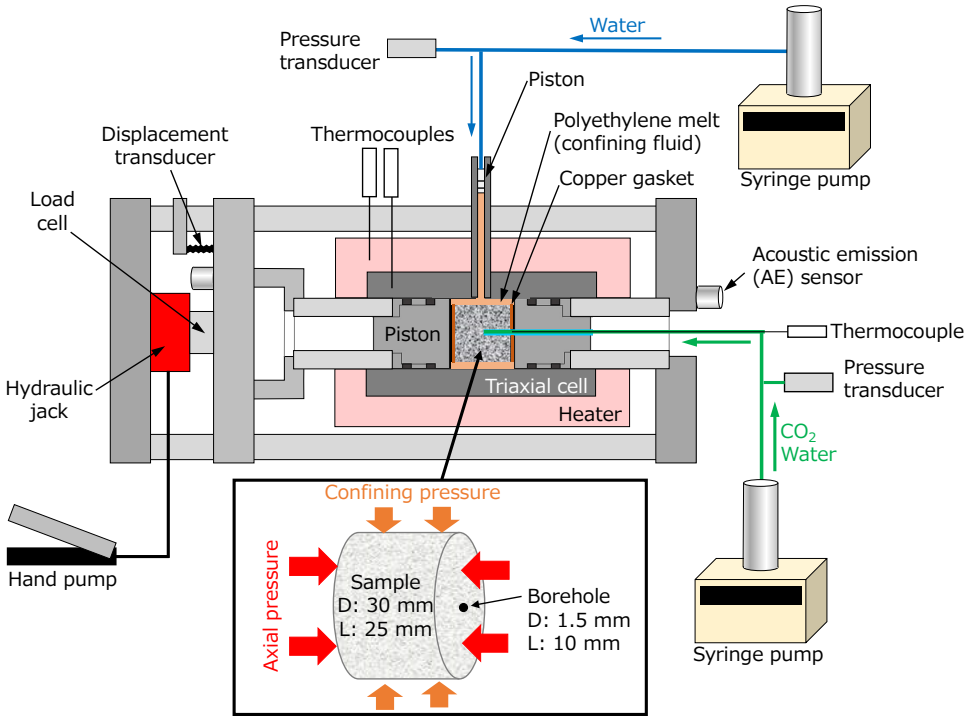

Figure 1. Experimental system.

For the experiment, the polyimide-film-wrapped sample was first placed inside the PE cylinder within the triaxial cell. The gaskets were attached to the end faces of the sample. The triaxial cell was then placed inside the electric furnace, and at a relatively small axial pressure maintained by a hydraulic jack, the temperature was increased to 250 °C, melting both the PE cylinder and the bottom part of the PE rod. The sample was then subjected to an axial pressure of 80-100 MPa, and a confining pressure of 30 MPa. Throughout the experiments, the fracturing fluid in the syringe pump was injected at a constant flow rate of 1 mL/min at room temperature. Injection was started after keeping 10-MPa borehole pressure for approximately 20 min. At such initial pressure, CO_2 existed in the liquid phase within the syringe pump at room temperature, enabling flow rate control even for CO_2. The injected fracturing fluid was heated to the experimental temperature in the injection pipe before delivery to the face of the sample.

Table 1 lists the rock type, fracturing fluid, temperature, confining pressure, and axial pressure in each experiment conducted. To investigate differences between water and CO_2 fracturing, water and CO_2 fracturing experiments were conducted on samples prepared from all rock types (Runs 1-4). As a result, it was confirmed for all rock types that fracture opening/propagation tended to be suppressed in CO_2 fracturing due to the low viscosity of CO_2. It should be noted that, at 250 °C and 10 MPa, the viscosities of CO_2 and water are 26 μPa·s and 110 μPa·s, respectively. Consequently, to investigate possibility to overcome this drawback in CO_2 fracturing, an additional fracturing experiment (Run 5) was conducted on a sample prepared from the andesite, in which 10-MPa CO_2 existed in the borehole and injection pipe was pushed into the sample by water. In this experiment, it was expected that low-viscosity CO_2 created fractures first, and then high-viscosity water opened and propagated the fractures.

Table 1. Rock type, fracturing fluid, temperature, confining pressure, and axial pressure in each experiment.

Experiment	Rock type	Fracturing fluid	Temperature (°C)	Confining press. (MPa)	Axial press. (MPa)
Run 1	Andesite	Water	250	30	100
Run 2	Andesite	CO_2	250	30	100
Run 3	Basalt	Water	250	30	80
Run 4	Basalt	CO_2	250	30	80
Run 5	Andesite	CO_2 and water	250	30	100

3 RESULTS AND DISCUSSION

Figure 2 compares changes in borehole pressure and AE energy with time between water and CO_2 fracturing experiments on the andesite (Runs 1 and 2). It should be noted that AE energy tends to be larger for a larger area of fracture propagation per unit time. In Run 1, a large-energy AE occurred instantaneously around 250 s or at a borehole pressure of approximately 70 MPa, after which only much smaller-energy AE occurred instantaneously. Consequently, fracturing in Run 1 initiated and ceased in a short time. In contrast, in Run 2, large-energy AEs started to occur non-instantaneously and frequently at around 260 s or at a smaller borehole pressure of approximately 40 MPa. Additionally, AE energy was generally smaller for Run 2. It should be noted that AEs before 260 s were considered not to be caused by fracturing because of their long intervals. Such earlier AEs may have been caused by deformation of the rock due to elevated pore pressure by infiltration of low-viscosity CO_2. These indicated that CO_2 fracturing initiated at a lower borehole pressure, and continued for a longer time, where a large, linear fracture extending from the borehole to the sample surface was not created instantaneously.

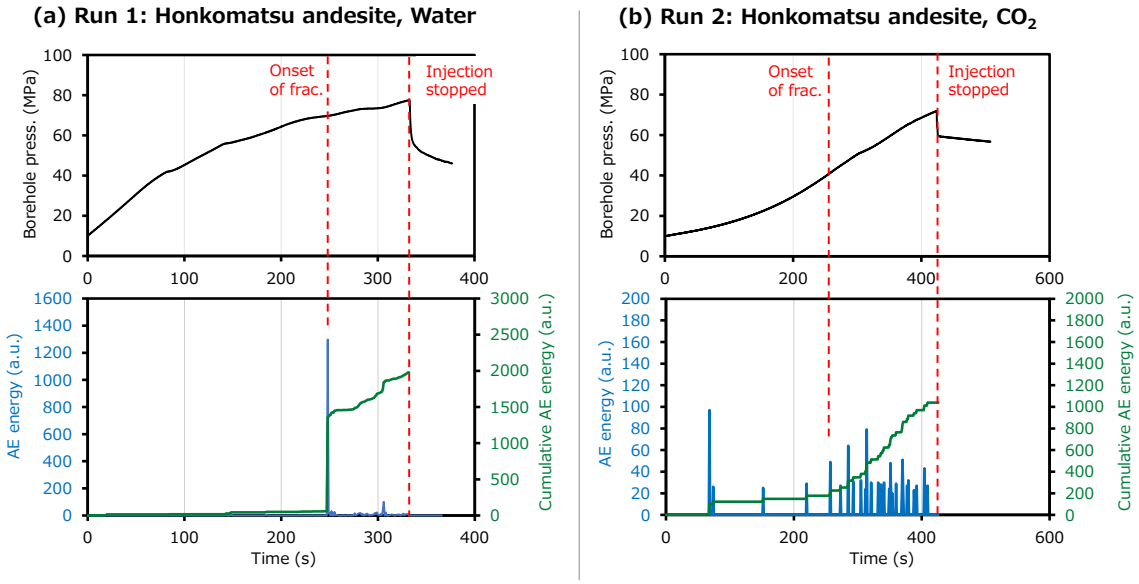

Figure 2. Changes in borehole pressure and AE energy with time in Runs 1 (a) and 2 (b).

Figure 3 shows fracture patterns which were visible in X-ray CT images taken after Runs 1 and 2. The shape of the yellow curve approximates shape of the fracture. It should be noted here that the fractures by water fracturing in Runs 1 and 3 tended to have larger apertures compared to that by CO_2 fracturing in Runs 2 and 4. The fractures in Run 1 were fewer and more linear. The permeability of the sample in Run 1 was increased from 4×10^{-18} m^2 to 3×10^{-17} m^2. In contrast, the fractures in Run 2 were larger in number and more tortuous. The permeability of the sample in Run 2 was increased from 1×10^{-18} m^2 to 1×10^{-16} m^2. The differences in the AE energy between Runs 1 and 2 may have reflected the differences in the fracture pattern between these two experiments.

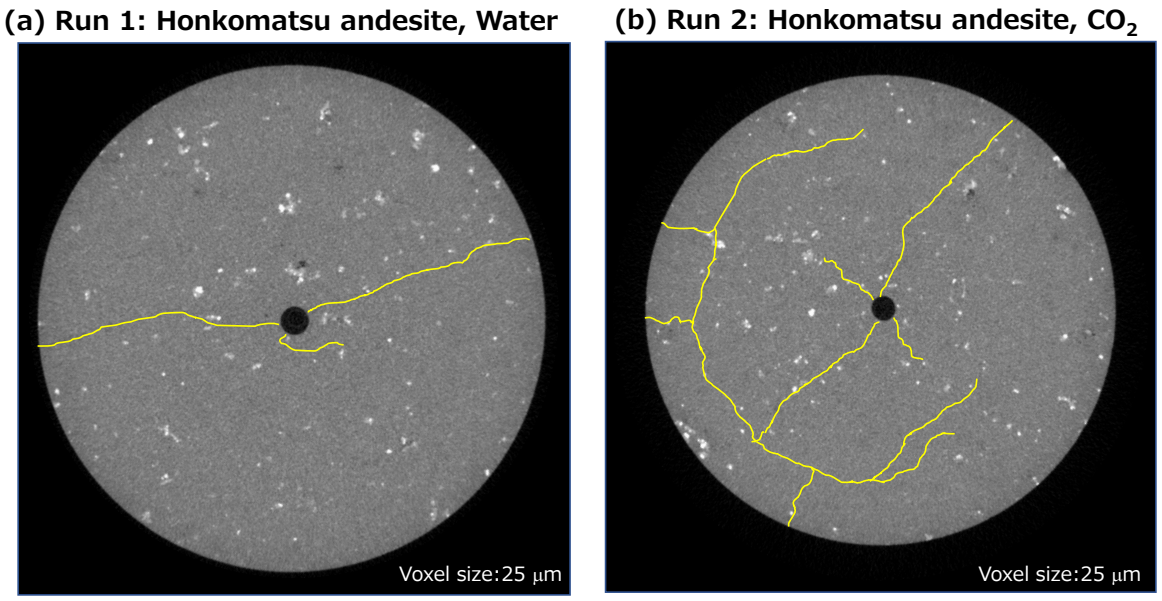

Figure 3. Fracture patterns which were visible in X-ray CT images taken after Runs 1 (a) and 2 (b). Fractures are highlighted by yellow.

Results in Runs 3 and 4 on the basalt (figures are not shown in this paper) were qualitatively similar to those in Runs 1 and 2, respectively. Based on the results in Runs 1-4, CO_2 fracturing has the advantage of producing a more complex fracture pattern at a lower injection pressure but has the

disadvantage of smaller fracture aperture. In contrast, water fracturing has the advantage in producing larger-aperture fracture, and the disadvantage in producing a less complex fracture pattern at a higher injection pressure. Since the difference in the experimental conditions between Runs 1 and 2 or between Runs 3 and 4 was only the fracturing fluid, the differences between water and CO_2 fracturing characteristics may have been caused by the difference between water and CO_2 viscosities. That is, low-viscosity CO_2 may have infiltrated into the rock and elevated pore pressure (i.e., reduced effective stress) to initiate fracture at a lower borehole pressure. Additionally, even after the initiation of fracture, pore pressure in the rock may have continuously increased and reduced a fluid pressure difference between inside and outside of the fracture to inhibit fracture opening/propagation, and to allow fracture initiation at another location. Moreover, such fracturing process accompanied by CO_2 infiltration may have altered the stress filed continuously to induce fracture tortuosity. Consequently, it was expected that the disadvantage in CO_2 fracturing was removed by injecting water into a rock after creating fractures by CO_2 to open/propagate the fractures by water, as demonstrated in Run 5 as described below.

Figure 4 shows changes in borehole pressure and AE energy with time in Run 5, and X-ray CT image taken after the experiment. Changes in AE energy in this experiment was similar to that in Run 2 of CO_2 fracturing on the same type of rock. The AE data indicated fracturing in Run 5 was initiated at a borehole pressure of approximately 30 MPa, which was also smaller than that in Run 1 of water fracturing on the same type of rock. It should be noted that water arrived at the borehole at approximately 240 s in the present experimental system. The fracture pattern in Run 5 was complex, and consisted of longer, larger-aperture fractures extending from the borehole, and dispersed short, smaller-aperture fractures. The fracture aperture in Run 5 was generally larger than that in Run 2, and the sample permeability in Run 5 was unmeasurably high (i.e., the sample was separated into several parts by fractures). The dispersed fractures were not visible in X-ray CT image in Run 2. However, such fractures should have been also created in Run 2 although the aperture of such fractures were too small to detect with X-ray CT, because the AE activities in Runs 2 and 5 were similar. Consequently, it was implied that, in Run 5, smaller-aperture fractures were created at many locations by CO_2 first, then these fractures were opened/extended by water.

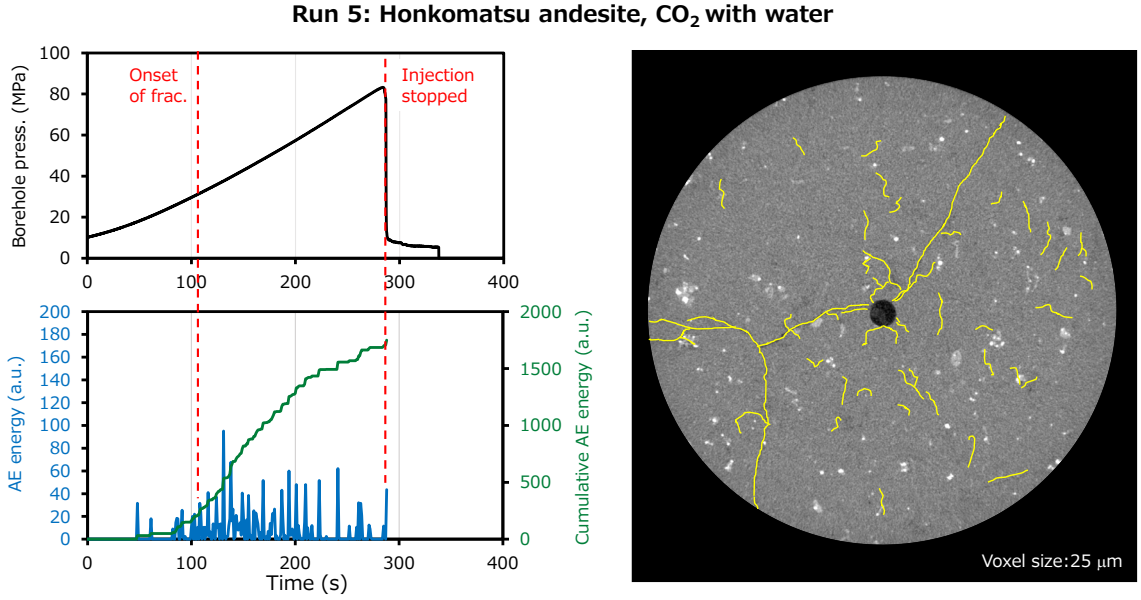

Figure 4. Changes in borehole pressure and AE energy with time in Run 5, and X-ray CT image taken after the experiment. Fractures that are visible in the image are highlighted by yellow.

4 CONCLUSIONS

CO_2-based enhanced geothermal system that uses CO_2 for both reservoir creation and thermal energy extraction has been attracting attention in Japan. For this system, CO_2 is injected into low-permeability reservoirs such as volcanic rock reservoirs to create highly permeable fractures. However, there has been no previous study on CO_2 fracturing of volcanic rocks under geothermal conditions so far. Possibility and characteristics of such CO_2 fracturing has thus been experimentally investigated in this study.

The results of CO_2 fracturing experiments on andesite and basalt at 250 °C and a confining pressure of 30 MPa have demonstrated that CO_2 fracturing occurs at a lower pressure than water fracturing and produces a more complex fracture pattern with a substantial permeability improvement, although there is the disadvantage of smaller-aperture fracture. Additionally, the present study has revealed that CO_2 fracturing with water, in which CO_2 is chased and pressurized by water, can produce larger-aperture fractures (i.e., larger permeability improvement) with keeping the advantage in CO_2 fracturing.

ACKNOWLEDGEMENTS

This study was partially supported by the Japan Society for the Promotion of Science (JSPS) through Grants-in-Aid for Scientific Research (B) (no. 22H02015), Challenging Research (Pioneering) (no. 21K18200). The authors would like to thank Toei Scientific Industrial Co., Ltd. for manufacturing the experimental system.

REFERENCES

Goto, R., Watanabe, N., Sakaguchi, K., Miura, T., Chen, Y., Ishibashi, T., Pramudyo, E., Parisio, F., Yoshioka, K., Nakamura, K., Komai, T. & Tsuchiya, N. 2021. Creating cloud-fracture network by flow-induced microfracturing in superhot geothermal environments. *Rock Mechanics and Rock Engineering* 54, pp. 2959–2974.

Isaka, B.L.A., Ranjith, P.G., Rathnaweera, T.D., Wanniarachchi., W.A.M., Kumari, W.G.P. & Haquea, A. 2019. Testing the frackability of granite using supercritical carbon dioxide: Insights into geothermal energy systems. *Journal of CO_2 utilization* 34, pp. 180-197.

Pramudyo, E., Goto, R., Sakaguchi, K., Nakamura, K. & Watanabe, N. 2023. CO_2 injection-induced shearing and fracturing in naturally fractured conventional and superhot geothermal environments. *Rock Mechanics and Rock Engineering* 56, pp. 1663–1677.

Pramudyo, E., Goto, R. Watanabe, N., Sakaguchi, K., Nakamura, K. & Komai, T. 2021. CO_2 injection-induced complex cloud-fracture networks in granite at conventional and superhot geothermal conditions. *Geothermics* 97, Article number: 102265.

Watanabe, N., Abe, H., Okamoto, A., Nakamura, K. & Komai, T. 2021. Formation of amorphous silica nanoparticles and its impact on permeability of fractured granite in superhot geothermal environments. *Scientific Reports* 11, Article number: 5340.

Watanabe, N., Egawa, M., Sakaguchi, K., Ishibashi, T. & Tsuchiya, N. 2017a. Hydraulic fracturing and permeability enhancement in granite from subcritical/brittle to supercritical/ductile conditions. *Geophysical Research Letters* 44, pp. 5468-5475.

Watanabe, N., Numakura, T., Sakaguchi, K., Saishu, H., Okamoto, A., Ingebritsen, S.E. & Tsuchiya, N. 2017b. Potentially exploitable supercritical geothermal resources in the ductile crust. *Nature Geoscience* 10, pp. 140-144.

Watanabe, N., Saito, K., Okamoto, A., Nakamura, K., Ishibashi, T., Saishu, H., Komai, T. & Tsuchiya, N. 2020. Stabilizing and enhancing permeability for sustainable and profitable energy extraction from superhot geothermal environments. *Applied Energy* 260, Article number: 114306.